

FEDSM-ICNMM2010-31330

OBSERVING HUMAN BLOOD CELLS IN FLOW THROUGH MICROCHANNELS

Harry L. Goldsmith

Department of Medicine, McGill University
Montreal, Quebec, Canada

ABSTRACT

For the rheologist, blood is essentially a concentrated suspension of biconcave 8- μm diameter red cells (40 - 45% by volume) that circulates within the body in vessels from 25 mm down to 5 μm diameter. Here, we describe in vitro tracking of blood cells in a traveling microtube apparatus and in a counter-rotating micro cone-plate device at low Reynolds numbers, Re . Observations of the flow behavior of individual red cells reveal a marked and continuously changing deformation and interaction of the cells in shear, and this, together with their migration away from the vessel wall accounts for the low whole blood overall viscosity compared to other concentrated suspensions and emulsions. Red cells also strongly affect the flow behavior and interactions of platelets and of white cells, which although present at much lower concentrations (0.3% by volume), play key roles in thrombosis, hemostasis, and inflammation. Studies of the kinetics of the formation and break-up of receptor-ligand bonds between membranes of platelets and of white cells in shear flow revealed single bond strengths of 50 -200 nN. Such micro particle image velocimetry (μPIV) studies have recently been considerably refined and extended to in vivo vessels such as postcapillary venules. Using submicron fluorescent latex spheres, the existence of an impermeable and hydrodynamically effective surface layer ($< 0.5 \mu\text{m}$ thick) extending out from the vessel endothelium has been confirmed. The lecture is illustrated by movies of blood flow in vitro and in vivo.

1 INTRODUCTION

In the last 15 years there have been considerable advances in tracking the motions of micro- and nano-sized particles suspended in fluids and tissues. Depending on the objective of the work and the systems studied, the methodology has been described as particle or micro-particle tracking velocimetry, fluorescent micro-particle velocimetry, particle or multi-particle velocimetry, particle or multi-particle tracking microrheology or velocimetry, and bio-microrheology. Actually, particle tracking has a much older history. The term microrheology was originally coined in

1960 by my thesis supervisor at McGill, Stanley Mason (1914-1987). As we wrote in the chapter in Eirich's Rheology Vol. IV, the task of microrheology is to predict the macroscopic rheological properties of a material from a detailed description of the elements of which it is composed [1]. Mason, working at the Pulp and Paper Research Institute at McGill, realized that to understand the manner in which an aqueous suspension of wood pulp fibers behaves in the papermaking process, one had to start observing the motions of individual particles. Starting much lower on the scale of complexity, he began by studying the behavior of isolated rigid spheres and cylinders in a simple shear flow [2-5]. Particle motions and interactions were observed under a microscope keeping the elements in the field of view and taking 16 mm movies. Such experiments on particle tracking had never before been attempted nor had anyone succeeded in building Couette and 4-Roller flow devices in which millimeter or micrometer sized particles could be observed and photographed while the rate of shear was varied at will. The first paper on the rotation of glass spheres and cylinders was published in 1951 [2].

When I arrived on the scene in 1958, Mason was interested in studying particle flow behavior in Poiseuille flow and in the subject of axial migration in tube flow. Physiologists had for years described the existence of a red cell-depleted layer at the periphery of blood vessels. A device was built in which a microscope and attached movie camera travelled along the length of vertically mounted fixed tubes (2 – 8 mm I.D.). Rigid spheres, discs, rods and fluid drops could be tracked in steady or pulsatile flow at low Re . Carefully designed single particle experiments and fluid mechanical theory showed that fluid drops, suspended in immiscible oils, when deformed into ellipsoids in shear flow migrate towards the tube axis [6], and so did deformable fibers [7]. Would it also apply to red blood cells?

2 TRACKING HUMAN RED BLOOD CELLS (RBC)

The technique was miniaturized by constructing a traveling microtube [8,9] in which the tube (50 – 200 μm I.D.), the supporting microscope slide and the infusion and collecting reservoirs move in a direction opposite to that of the flowing cell under observation, (Fig. 1).

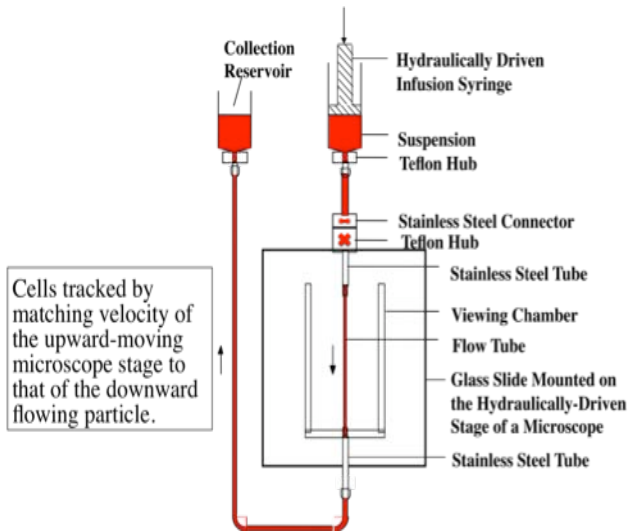


Fig. 1: Schematic diagram of the vertically-mounted traveling microtube. The device consists of a vertically mounted, sliding platform supporting a syringe infusion pump and having a built-in microscope stage on which was mounted the flow tube lying on a microscope slide. Both infusion pump and platform are hydraulically driven. The optic axis of the microscope is fixed and normal to the platform

2.1 RBC Rotation and Deformation

At low hematocrits and shear stress, $\tau < 0.03$ Pa, single RBC rotate with periodically varying angular velocities as rigid oblate ellipsoids or discs [8,10] while maintaining their biconcave shape. As $\tau > 0.03$ Pa the rotational motion deviates from theory, the cells spending more time aligned with the flow. Above a critical τ , the cell rotational motion ceases, and they align themselves with the flow with the membrane rotating about the cell interior, as would be the case for a fluid drop. Such behavior, first observed for RBC in isotonic Dextran solutions [11] is shown in Fig. 2B for RBC in 30% Dextran having $40 \times$ the viscosity of plasma. Two-dimensional theory in simple shear predicts that cell deformation and membrane rotation are functions of the applied shear rate, G , and viscosity ratio internal:external phase viscosity [12].

2.2 Rouleau Rotation and Deformation

Linear rouleaux of red cells having more than 6 cells exhibited bending and cell deformation during the rotational orbit. At a given G , the degree of bending increased with the number of cells. Figure 3 shows the rotation of an 11 and a 16 cell rouleau drawn from cine-photomicrographs at 5 positions.

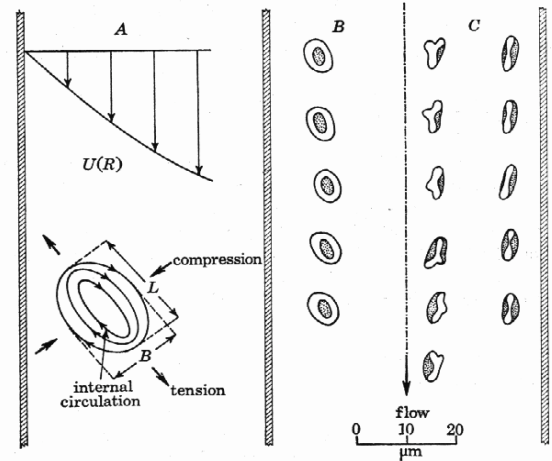


Fig. 2: A: 2-mm diam. water drop in viscous oil deformed into an ellipsoid with internal circulation, $G = 1 \text{ s}^{-1}$. B: Human RBC in isotonic Dextran, $\eta = 54 \text{ mPa s}$ deformed into an ellipsoid-like shape at successive times in flow down the tube, $G = 1.8 \text{ s}^{-1}$. C: The same suspension showing a cell (left) that had become more rigid, and right a cell at higher $G = 4.7 \text{ s}^{-1}$ still aligned but oriented out of the median plane. From [8] with permission.

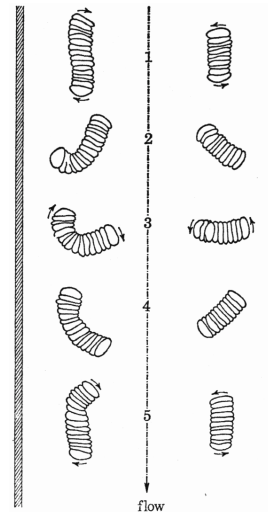


Fig. 3 Rotation of an 11- and a 16-cell rouleau in Poiseuille flow at shear rates $< 20 \text{ s}^{-1}$ in an $83\text{-}\mu\text{m}$ diameter tube. Tracings of the rouleaux from cine-photomicrographs during one half orbit between positions 1 and 5 showing bending during rotation in the quadrants under compressive normal fluid stresses (position 2), accompanied by distortion of individual RBC in the chain. The rouleaux tended to straighten out in the next quadrant under tensile stresses (position 4). Such “springy orbits” had previously been observed with model nylon, dacron, and rayon filaments [13]. After [8] with permission

2.3 Radial Migration of RBC

The vessel boundary has an effect not only on both the rotational and translational velocities of particles within one or two cell diameters from the wall, but also by generating radial components of velocity. Two mechanisms operate for particle migration in tube flow:

(a) *Migration due to particle deformation.* Fluid drops and flexible fibers, suspended in Newtonian media undergoing Poiseuille flow in the creeping flow regime, migrate towards

the tube axis [6,14,15]. Rigid particles do not migrate. Single red blood cells and rouleaux under conditions of negligible fluid inertia migrate radially inward, whereas aldehyde-fixed, rigid RBC do not migrate, Fig. 4 [16].

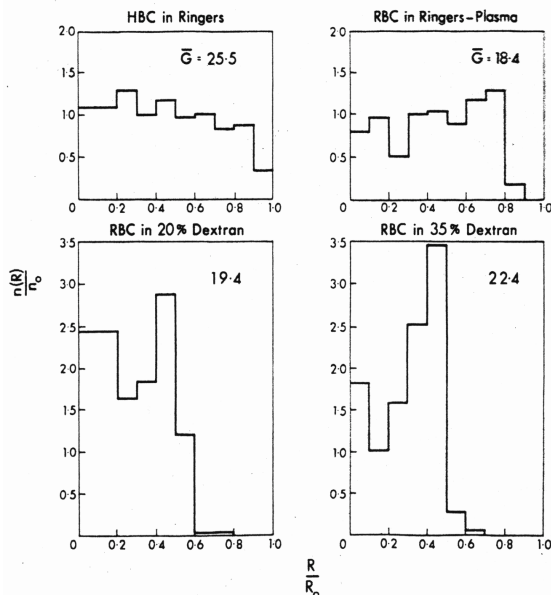


Fig. 4. Number concentration distribution of normal (RBC) and glutaraldehyde-hardened red cells (HBC) in an 83 μm diameter tube, 1 cm downstream of its entry from a reservoir. Plot of the number of cells/ cm^3 $n(R)$, at intervals of one tenth tube radius (R_0) divided by the number/ cm^3 in the reservoir, n_0 , against the dimensionless radial distance R/R_0 . For uniform concentration of cells across the tube $n(R)/n_0 = 1$. It is evident that the deformable RBC undergo appreciable migration away from the wall, especially in the more viscous dextran solutions. By contrast, the rigid HBC are fairly uniformly distributed across the tube except close to the wall where no particle centers can approach closer than $\sim 3 \mu\text{m}$. From [16] with permission.

(b) *Migration due to inertia of the fluid.* At higher Re, there is a two-way lateral migration seen with rigid spheres and cylinders [tubular pinch effect, 17,18]. Rigid RBC in low viscosity Ringers solution at higher Reynolds numbers exhibit the tubular pinch effect, as do normal red cells, but the equilibrium position of the latter is closer to the tube axis than that that for rigid cells [16].

The relevance of radial migration of RBC due to deformation or inertia of the fluid as in the tubular pinch effect is discussed below in the section on cell flow behavior in whole blood.

3 FLOW BEHAVIOR OF RBC IN WHOLE BLOOD

In order to observe the motions of RBC in flowing blood at normal hematocrits, it was necessary to render the blood transparent to transmitted light. This was achieved by subjecting red cells to sudden osmotic lysis using hypotonic phosphate buffer and then reconstituting them by restoring the normal ionic strength of blood. The resulting ghost cells were then resuspended in the plasma when they were found to resume a biconcave shape [19]. Tracer red cells, platelets or white cells were then added, and their

motions in flow of 10 – 91% by volume of ghost cells were clearly visible. Studies of tracer cells in tubes of diameters from 60 – 150 μm at flow rates, Q , from 0.3 - 43 $\mu\text{L s}^{-1}$ [19] revealed non-Newtonian flow behavior similar to that observed in concentrated oil-in-oil emulsions [19-21].

3.1 Blunting of the Velocity Distribution

At ghost cell concentrations $> 20\%$, the velocity profile were blunted from the parabolic with a central region of plug flow in which the tracer RBC traveled with maximum and identical velocities, $u_M < U(0)$, the centerline velocity in Poiseuille flow at the same Q . As with oil-in-oil emulsions [21], at a given concentration and tube radius R_0 , the degree of blunting decreased with increasing Q (Fig. 5B), in striking contrast to the velocity distributions observed in concentrated suspensions of rigid discs and spheres, in which the velocity profile and degree of blunting are independent of the flow rate at very low Re [22]. The difference is due to the deformability of the oil droplets and that of the ghost and red cells, that increases with increasing fluid stress as Q increases. The remarkable deformation of RBC at ghost cells concentrations $\geq 40\%$ is discussed below.

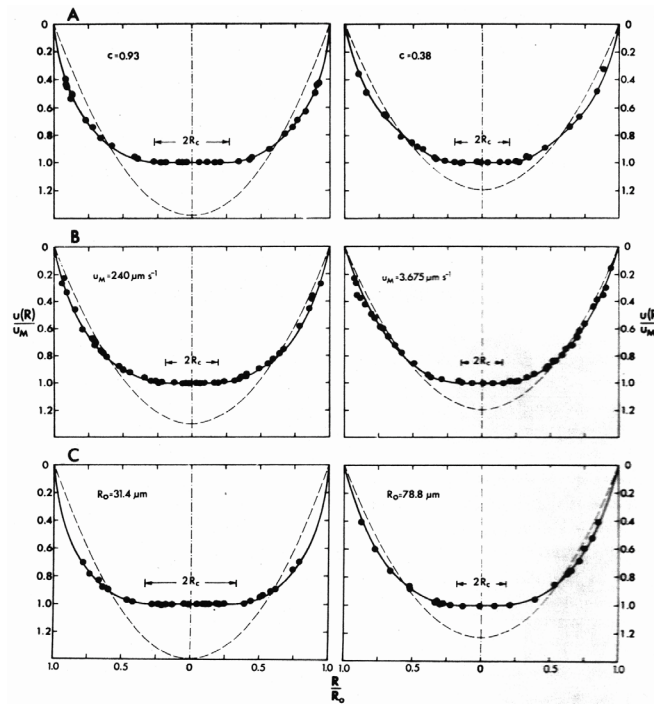


Fig. 5. Blunting of the velocity distribution in a transparent suspension of ghost cells in plasma. Plot of the dimensionless tracer cell velocity $u(R)/U(0)$ vs relative tube radius R/R_0 , showing the effect of A: ghost cell concentration $c = 93\%$ left and 38% , right; B: flow rate at $c = 43\%$, $Q = 8.8 \times 10^{-4}$ left and $5.36 \times 10^{-3} \mu\text{L s}^{-1}$ right; and C: tube radius $R_0 = 31.4$ and $78.8 \mu\text{m}$, respectively, $c = 0.60$. Solid lines are the best fit through the experimental points; the dashed lines are the parabolic distribution that would have been observed in Poiseuille flow. The difference between $U(0)$ and u_M reflects the degree of blunting of the velocity profile. From [19] with permission.

It should be noted that the blunting observed at low Re in the absence of inward migration in concentrated suspensions of rigid or deformable spheres and normal RBC is due to particle crowding [23].

3.2 Deformation of RBC due to shear and particle crowding

In flowing concentrated emulsions the drops are distorted from prolate ellipsoids into irregular shapes [21]. The distortions of the tracer RBC in ghost cell suspensions $>40\%$ by volume are even more striking and unlike the emulsion droplets, are seen even at very low shear stresses (< 0.03 Pa) at which isolated RBC in dilute suspensions of plasma undergo periodic angular rotation without deforming [8]. As seen in Fig. 6 at 55% by volume of ghost cells, the RBC spend much of their time aligned with the flow. The membrane may rotate about the interior in an irregular mode [19].

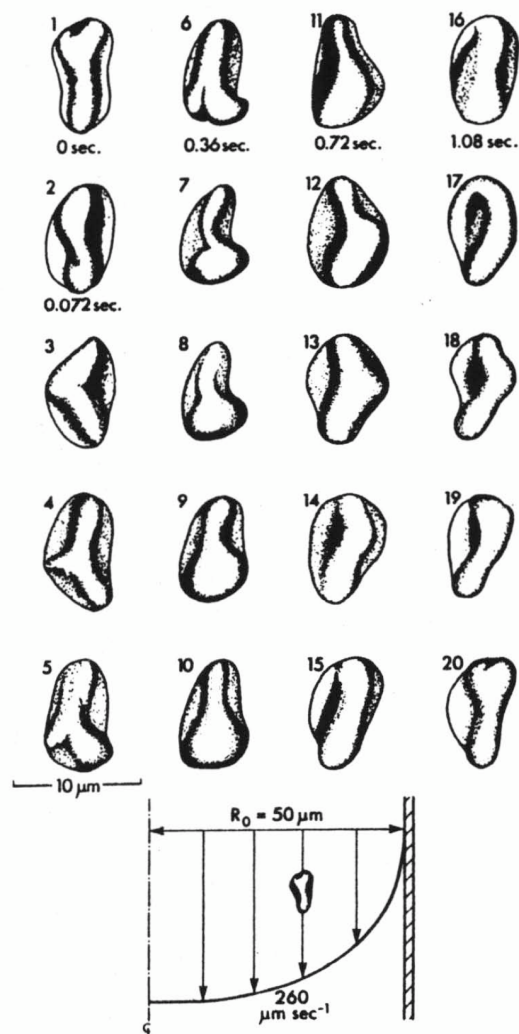


Fig. 6. Tracings from photomicrographs of the successive deformations of a tracer RBC in a 55% ghost cell suspension flowing through a 100 μm diameter tube. The cell, situated at a radial distance $R \sim 0.6R_0$, traveling at $260 \mu\text{m s}^{-1}$ is shown at 7.2 ms intervals, almost always aligned in the direction of flow. From [24] with permission.

The ability of human and many other mammalian red cells to deform and squeeze past each other in flow is likely to be the major reason for the remarkably low viscosity of whole blood at moderate and high shear stresses – see Fig. 7, below, that compares the relative viscosity of whole blood as a function of RBC concentration (hematocrit) with that of suspensions of rigid spheres, discs and emulsion droplets.

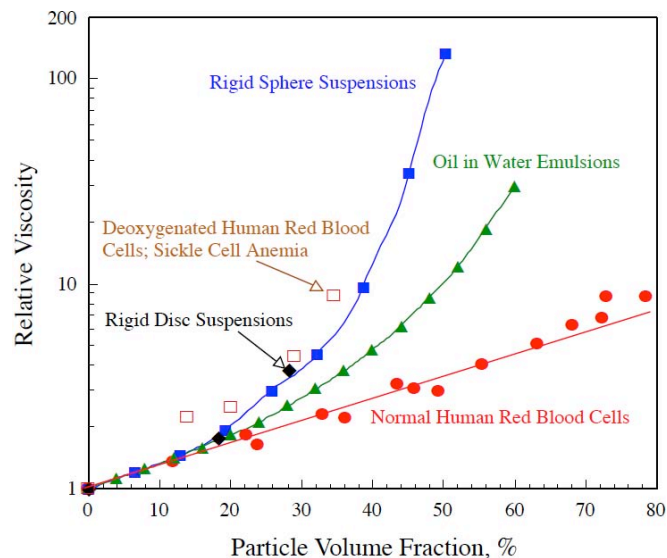


Fig. 7. Relative viscosity (viscosity of the suspension/viscosity of suspending phase fluid) of human red cells in plasma at shear rates $> 100 \text{ sec}^{-1}$ (●) as a function of particle volume fraction (hematocrit) compared to suspensions of rigid spheres (■) and rubber discs in glycerol (◆), and emulsions of deformable oil droplets in water (▲). Note the striking effect of a change of shape and rigidity on red cell viscosity for sickled cells (□).

3.3 Convective dispersion of cells

In view of the observed migration of red cells away from the tube wall (Fig. 3), one might expect a significant reduction in cell concentration at the vessel periphery even at normal hematocrit. However, it is unlikely that, in microvessels $\sim 100 \mu\text{m}$ diameter, such a cell-depleted zone is larger than $5 \mu\text{m}$ in width. The resistance to crowding at normal hematocrits opposes any appreciable inward cell migration, such as occurs at lower hematocrits. At the microscopic level, the resistance to crowding is seen as a series of continuous collisions between deformed red cells and the surrounding plasma, as illustrated for red cells in Fig. 8. Measurements of the mean square radial fluctuations of the paths of tracer red cells and $2 \mu\text{m}$ diameter latex spheres in ghost cell suspensions at $G \leq 30 \text{ s}^{-1}$ were used to compute dispersion coefficients. These were found to be two orders of magnitude greater than the Brownian translational diffusion coefficients of the particles in plasma [16,19]. The dispersion coefficients were also in fair agreement with platelet diffusion coefficients obtained from measurements of their dispersion in flowing blood [25]. As a consequence of the radial fluctuations in the paths of the cells, there are

frequent cell-vessel wall collisions - an important mechanism for blood platelets to come into proximity with, and adhere to, damaged endothelium thereby repairing the wall and avoiding penetration of blood into the tissues.

When groups of tracer RBC were followed for long times in the plug flow region, while plotting their relative positions, upstream or downstream of a reference RBC, it was found that there existed a small but measurable velocity gradient at radial positions within the central core ~ 0.20 and 0.12 s^{-1} in the 77 and 155 μm diameter tubes, respectively, shown in the figure below.

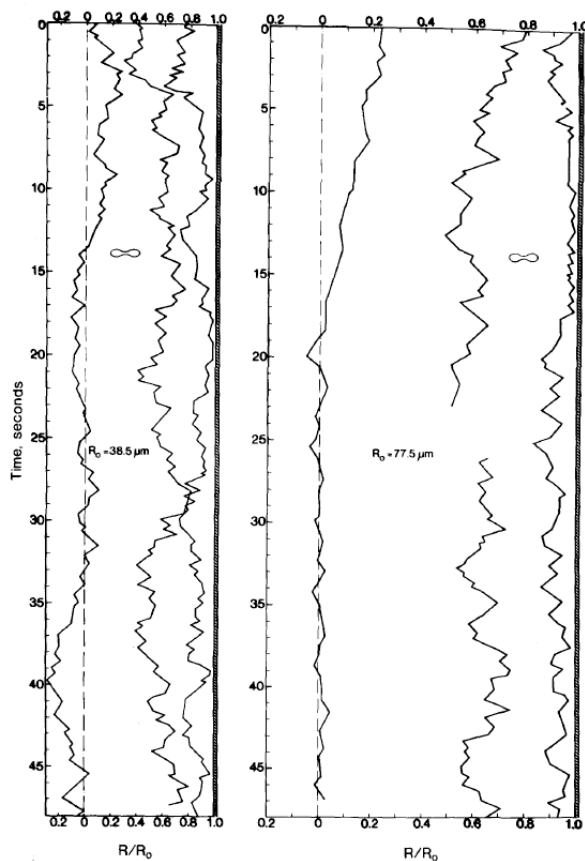


Fig. 8. Radial dispersion of the paths of tracer RBC in a 40% ghost cell suspension in flow through a 77 μm (left) and a 155 μm diameter tube (right). Plot of relative radial position vs time. RBC located between 0.4 and $0.8R_0$ had the largest radial displacements, the root mean square displacement being 3.32 and $3.84 \mu\text{m}$ in the 77 and $155 \mu\text{m}$ tubes respectively. For RBC near the tube axis they were 2.00 and $1.62 \mu\text{m}$, in the 77 and $155 \mu\text{m}$ tubes, respectively. In the 50 s sequences shown, the RBC in the periphery spent about 19% of the time in apparent contact with the wall. Note that the radial dispersion was transmitted into the central region of plug flow of zero measurable G : ~ 0.27 and $0.19R_0$ in the 77 and $155 \mu\text{m}$ tubes, respectively. From [19]. with permission.

3.4 Aggregation in whole blood at low shear stress

Paradoxically, the formation of a peripheral cell-depleted layer in vitro is much greater at low tube and wall shear rates when aggregates of RBC (rouleaux) are observed to form, than at higher

and physiologically representative shear rates in the absence of such aggregation. This happens despite the fact that net inwardly directed fluid mechanical forces depending on the deformation of the RBC, and the shear and normal fluid mechanical forces are much lower under slow flow conditions. Observations made in the traveling microtube show that, with decreasing flow rate, RBC aggregation into a network of rouleaux of rapidly increasing size occurs as the aggregates migrate away from the tube wall. At first there is still a velocity gradient in the axial network of rouleaux, but as the flow rate decreases further, a two-phase flow has developed. It consists of a large central compact network of aggregates of varying radius undergoing plug flow, surrounded by a peripheral layer consisting of single smaller rouleaux, white cells and platelets [26]. The latter were expelled from the red cell core into the periphery, a process called margination. The upper left panel of Fig. 9 (overleaf) shows measurements of the relative core radius r_c/r_o ($r_o =$ tube radius, $172 \mu\text{m}$) against flow rate \bar{U} (tube diameters/s) in 34% RBC suspended in buffered Dextran of 110 kDa Mol. Wt. It is evident that as $\bar{U} < 2.0$ a core of RBC of rapidly decreasing relative radius develops. At the same flow rate, the hydrodynamic resistance, $R =$ dynamic pressure drop/flow rate (lower left panel) that has been increasing with decreasing \bar{U} , now decreases as the core relative radius decreases. By contrast, the resistance of a suspension of RBC in a 10% serum albumin buffer in which there is no aggregation, continues to increase with decreasing \bar{U} .

The large standard deviations in the mean r_c/r_o (the bars in the graph) indicates that there are large variations in r_o along the length of the tube.

4 ADHESION OF BLOOD CELLS

Measuring the physical strength of the bonds linking biological cells to each other and to surfaces is important for characterizing adhesion processes that occur in the circulation and elsewhere, such as cancer metastasis, platelet thrombosis and leukocyte margination and extravasation in the venules of the microcirculation.

The development of the traveling microtube technique was now used to study two-body collisions between colloidal size latex spheres suspended in simple and polyelectrolytes [27,28]. It was shown that by cinefilm recording of the trajectories of the colliding particles one could compute the electrostatic repulsive and van der Waals attractive forces acting between sphere surfaces as these approach within 50 nm of each other.

4.1 Force to rupture receptor ligand bonds

Figure 10 shows 2 rigid spheres suspended in a liquid of viscosity η colliding with each other in a simple shear flow at a shear rate G near the wall of a vessel. A doublet forms, whose axis lies at an angle ϕ_1 to the X_2 -axis of the shear field: $u_1 = GX_2$, $u_2, u_3 = 0$, and at an angle θ_1 to the X_1 - or

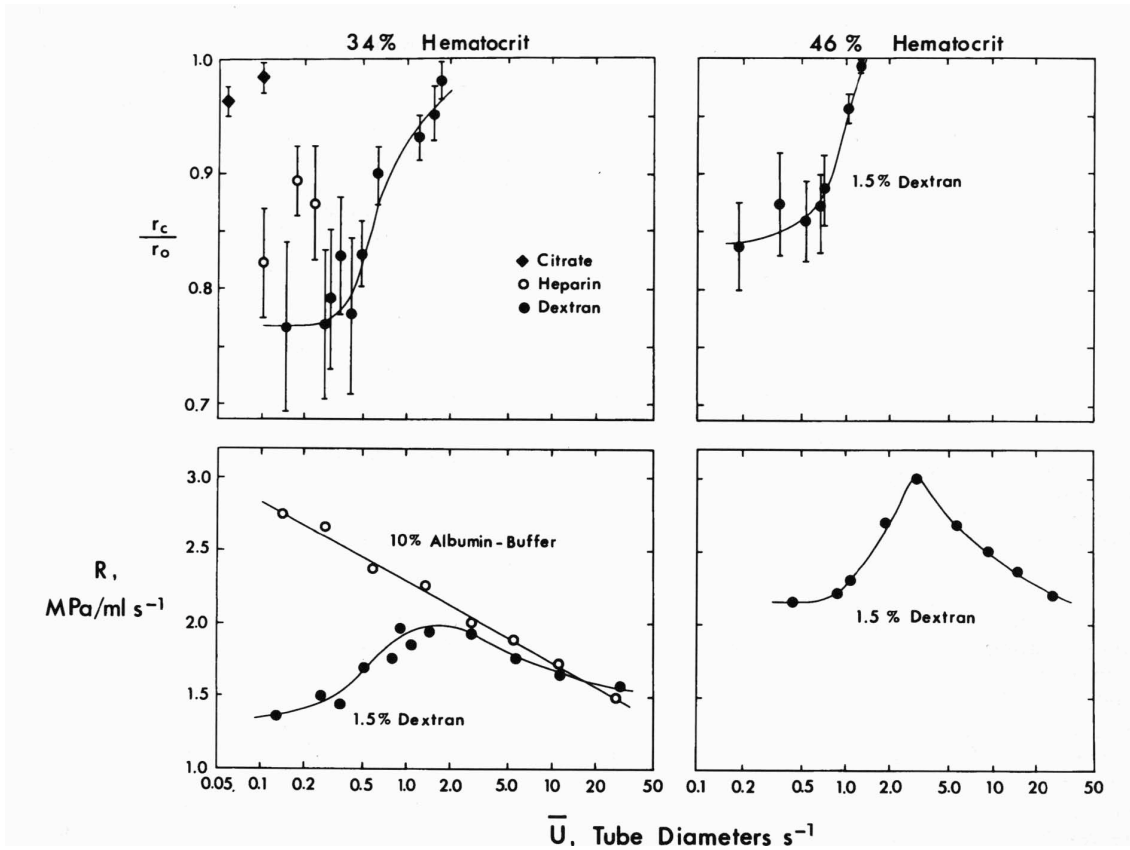


Fig. 9. Plots of the mean relative red blood cell core width, r_c/r_o , (upper panels) and hydrodynamic resistance, R (lower panels) as a function of linear flow rate \bar{U} at 34 and 46% hematocrit, $r_o = 172 \mu\text{m}$. Also shown are values of R obtained in a 10% albumin buffer (no RBC aggregation) and in citrated and heparinized blood where there is significantly less aggregation than in RBC dispersed in 1.5% Dextran 110. From [26], with permission.

vorticity axis. Sphere centers are separated by a distance s and sphere surfaces by a distance h . In the presence of an interaction force $F_{int}(h)$, the trajectory of the spheres is given by [29]:

$$\frac{3\pi\eta}{C(s^*)} \frac{ds}{dt} = \frac{A(s^*)}{C(s^*)} 3\pi\eta G b^2 \sin^2 \theta_1 \sin 2\phi_1 + F_{int}(h), \quad (1)$$

where $A(s^*)$ and $C(s^*)$ are known dimensionless functions of $s^* = s/b$. If a collision results in the formation of a permanent doublet due to a bond between receptors on adjacent spheres and a bivalent ligand, then if the doublet is rigidly linked, and with $ds/dt = 0$:

$$F_{int}(h) = \frac{A(s^*)}{C(s^*)} 3\pi\eta G b^2 \sin^2 \theta_1 \sin 2\phi_1 \quad (2)$$

Using a general method for calculating forces, torques and velocities of two interacting rigid neutrally buoyant spheres in shear flow [30], expressions for the normal force F_n acting along, and the shear force F_s acting normal to the axis of the doublet have been derived [31]:

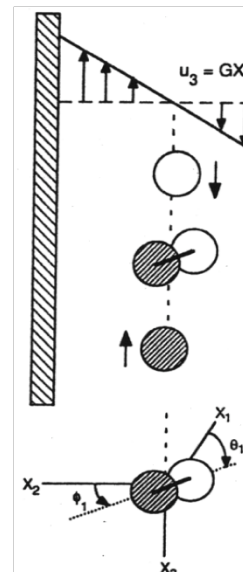


Fig. 10. 2-body collisions of equal-sized rigid spheres in simple shear flow, with origin at the center of rotation of the doublet. Coordinates (X_1, X_2, X_3) and (θ_1, ϕ_1) are constructed at the mid point of the doublet axis. From [32] with permission

$$F_n = \alpha_3(h)\eta G b^2 \sin 2\theta_1 \sin 2\phi_1 \quad (3)$$

$$F_s = \alpha_{12}(h)G b^2 \sin \theta_1 \times \left[\frac{\left(2\sin^2\theta_1 \cos^2\phi_1 - 1 \right)^2 \sin^2\phi_1 + \cos^2\theta_1 \cos^2\phi_1}{1 - \sin^2\theta_1 \cos^2\phi_1} \right]^{1/2} \quad (4)$$

where $\alpha_3(h)$ and $\alpha_{12}(h)$ are force coefficients, weakly dependent on the minimum distance of approach, h .

4.2 Force to break-up doublets of spheres cross-linked by ligand

Using a new model of the counter-rotating cone and plate rheoscope [33,34] we measured the time and force dependence of the break-up of doublets of sphered, swollen and fixed human red cells (SSRC) cross-linked by monoclonal IgM antibody in Couette flow [34]. It was shown that break-up is a stochastic process that can occur by extraction of antigen receptors from the cell membrane rather than by antigen-antibody break-up. We therefore prepared carboxyl-modified latex spheres having a covalently linked synthetic blood group B antigen trisaccharide [35]. We studied the shear-induced break-up of doublets of the antigen spheres cross-linked by monoclonal IgM antibody in buffered Dextran 40 (viscosity = 9.7 mPa s) to increase shear stress and reduce sedimentation of the spheres [35]. As can be seen in Fig. 11, there was a distribution in times to break up with the data binned into 4 force ranges. Break-up in the 2 lowest force ranges was very low (and not significantly different) but increased with increasing force, F_n with the upper 2 ranges being significantly different. The fraction of break-ups of the latex sphere doublets was lower than that of the SSRC doublets in Dextran.

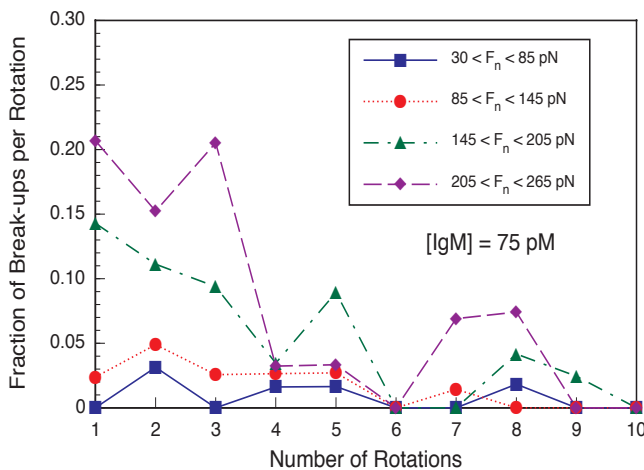


Fig. 11. Graph of fraction of breakups per doublet rotation: the fraction of the total number of doublets of antigen latex spheres cross-linked by monoclonal IgM observed in that rotation breaking up after onset of shear. Latex antigen spheres were suspended in 19% Dextran 40 and 75 pM IgM. Results were binned in 4 force ranges. From [35], with permission.

Computer simulation using a stochastic model of break-up [35] showed that the difference between the antigen sphere and SSRC doublet break-up was due to a change in bond character (the range and depth of the bond energy minimum) rather than to an increase in the number of bonds linking the antigen sphere doublets. This supports the notion that antibody-antigen bonds were ruptured in the case of the doublets of antigen latex spheres, but that antigen was extracted from the membrane of the SSRC.

4.3 Dynamics of neutrophil aggregation in Couette flow

During inflammation, neutrophil (PMN) capture by vascular endothelial cells is dependent on L-selectin and β_2 -integrin adhesion-receptor bonds. It has been shown that neutrophil aggregation is analogous to this process in that it is also mediated by these receptors, thus providing a model for PMN aggregation [36].

Suspensions of unstimulated human neutrophils in Tyrodes solution containing 5% or 10% Ficoll 400 (to increase its viscosity) were subjected to a uniform shear field in the rheoscope. Two-body collisions between cells and the formation of doublets and higher order multiplets at $G = 14 - 220 \text{ s}^{-1}$ were recorded with high speed video-microscopy. As shown in Fig. 12, when two rigid spheres collide in shear flow and form a doublet, it is subject to alternate normal forces (compression and tension) and tangential shear forces. The lifetime of the doublet of cells, when it is transient and separates under tensile force, or when non-separating due to bond formation, is a function of shear rate and shear stress. That bond formation had occurred during a collision was evident when doublets rotated intact well past the quadrant in which they were subject to tensile forces.

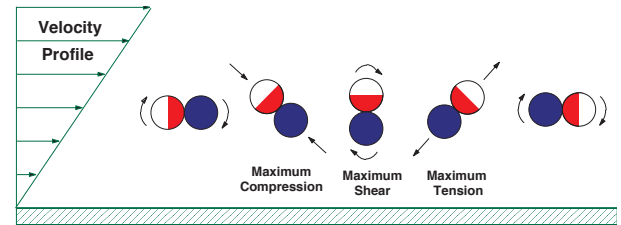


Fig. 12. Schematic diagram of the rotation of a non-separating doublet of rigid spheres in simple shear flow showing the maximum normal compression and tension forces at orientations of the axis of revolution (see Fig. 10) $\phi_i = 45$ and 135° , respectively, and maximum tangential (shear) force at $\phi_i = 90^\circ$.

(a) *Effect of shear rate and shear stress* [37]. The doublet lifetimes, τ_{meas} , relative to those predicted for neutral non-interacting spheres, $\tau_{theor} = 5\pi/6G$, and the collision efficiency (fraction of collisions resulting in the formation of non-separating doublets) increased with increasing shear rate, and at a given G with increasing shear stress. Figure 13 shows that both the rate and extent of aggregation increased with increasing shear rate over the first 10 s of shear, and Fig. 14 shows that the total extent of aggregation and the

size of the aggregates increased with shear rate and shear stress.

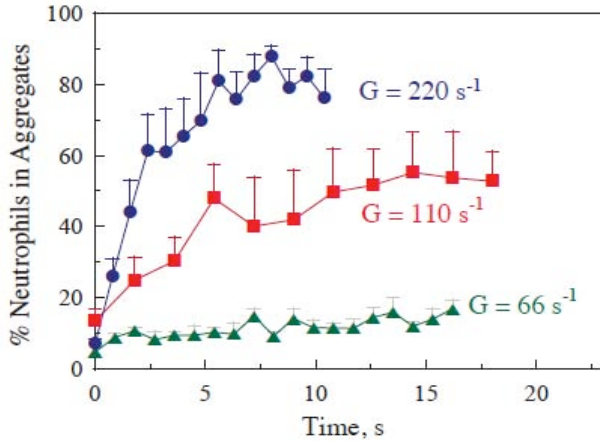


Fig. 13. Effect of shear rate on the rate neutrophil aggregation in a suspension of buffered 10% Ficoll ($\eta = 5.49 \text{ mPa s}$) containing 20,000 cells/ μL at the shear rates, G , shown. A marked increase in the rate and extent of aggregation was observed. From [37] with permission.

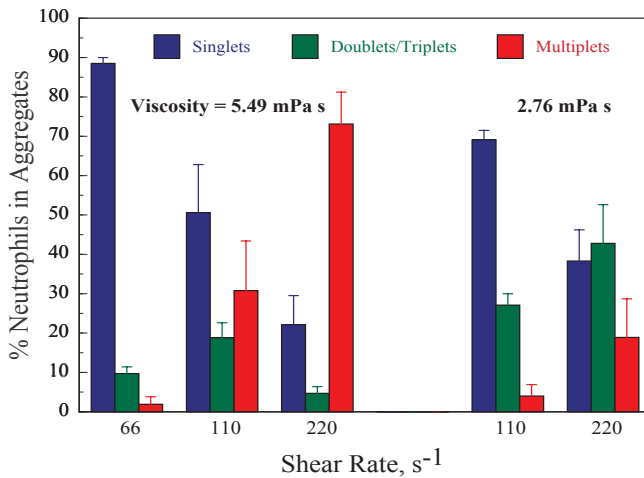


Fig. 14. Effect of shear rate and shear stress on the distribution of neutrophil aggregate size after 10.8 s of shear. Histograms of the mean fraction of neutrophils binned into singlets, doublets and triplets and higher-order multiplets. Note the rapid increase in the % neutrophils in multiplets in the more viscous 10% Ficoll at shear stresses from 0.36 at $G = 66 \text{ s}^{-1}$ to 1.2 Pa at 220 s^{-1} . From [37] with permission.

(b) *Aggregation requires maintenance of shear.* In the case of unstimulated neutrophils undergoing shear at $G \geq 66 \text{ s}^{-1}$, rapidly reducing G to 14 s^{-1} resulted in rapid and complete disaggregation, that in turn could be totally reversed by raising G back to its initial value [37]. The effect was completely absent in neutrophils that had been activated with $1 \mu\text{M}$ formyl met-leu-phe (fMLP), a strong chemoattractant.

(c) *Mechanism of shear dependence of aggregation.* The most likely mechanism for the existence of a threshold G for

aggregation to occur and be maintained is associated with the cell deformation of the doublet that occurs in the quadrant $0^\circ < \phi_l < 90^\circ$ during compressive normal force loading.

The time spent during the following quarter rotation ($90^\circ - 180^\circ$) under tensile force loading is computed to be 10.6 and 5.3 ms at $G = 110$ and 220 s^{-1} , respectively [37]. From biomembrane force probe experiments by Evans et al. [38], these times are significantly longer than the times for a single L-selectin-PSGL-1 bond to dissociate: ~ 1.5 and 0.2 ms at the mean normal forces of $F_n = 139$ and 278 pN , respectively. However, if multiple bonds were formed during the previous compressive normal force loading these times would increase as zipper like dissociation of bonds occurs. The opportunity for multiple bond formation would arise if flattening of the neutrophils occurred as the cells come into close proximity under a sufficiently high normal force and area of contact of $5 \mu\text{m}^2$ (of the total cell surface area = $240 \mu\text{m}^2$) were formed [38].

The question why does the cell not relax during the quadrants under tensile force is likely due to the neutrophil having a turgor pressure P_c of 10 N m^{-2} [39] and a high internal viscosity $\eta_{\text{PMN}} \sim 10 \text{ Pa s}$. The time to relax = P_c/η_{PMN} would then be 1 s compared to a mean time under tensile force, $< 10.6 \text{ ms}$. Thus, the neutrophil never has enough time to relax under force and the bonds remain intact. As for the finding that a threshold shear rate has to be exceeded for significant neutrophil aggregation to occur, that could be explained by the existence of a threshold rate of compression-force loading. Below the threshold, the rate of formation of the contact area is not rapid enough to allow sufficient number of bonds to form. Thus, in the 5% Ficoll at lower shear stress the doublet lifetimes, capture efficiencies and extents of aggregation are significantly lower than in the 10% Ficoll.

(d) *Tether formation.* The surface of the membranes of resting human neutrophils is ruffled and rich in projections called microvilli (Fig. 15). Supported by actin filaments they protrude from the spherical surface as tiny cylinders of the membrane. The receptor molecules L-selectin and its ligand P-selectin glycoprotein ligand-1 (PSGL-1) are localized in them [40]. When the neutrophil approaches the wall of a post-capillary venule, the tip of the microvillus is most likely to be the first point of contact [41], as a bond is formed between L-selection or PSGL-1 and P- and E-selectin on the venular endothelium. As the blood flow pushes the cell and it rolls along the endothelium, the bond or bonds (preferably located on the tip of the microvillus) experience a tensile force that is known to shorten their lifetime, or even extract receptor or ligand from the cell surface. It has been shown in static experiments that under tensile forces $> 64 \text{ pN}$ the microvillus anchorage point will stretch up to $1.9 \mu\text{m}$ length [41]. In the experiments described in section 4.3(a), the maximum tensile forces at $G = 110$ and 220 s^{-1} were much greater than 64 pN . Following compression, there might then

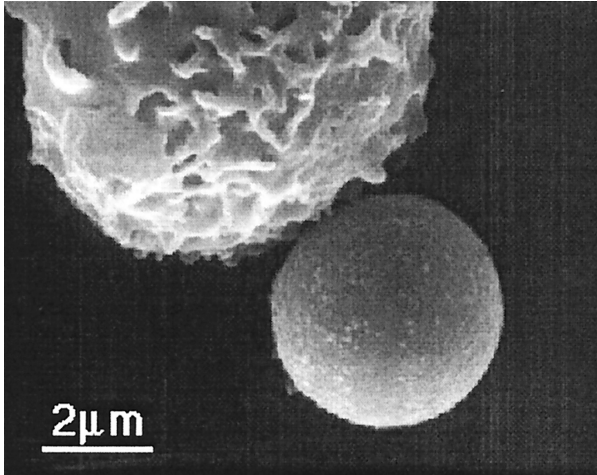


Fig. 15. Scanning electron micrograph showing half of a human neutrophil with typical ruffled surface showing the tips of microvilli through two of which the cell is adhering to a latex bead coated with anti-CD45. From [41] with permission.

be stretching of the microvillus during rotation from $\phi_1 = 0^\circ$ to 90° , resulting in tether formation. However, this would be much less likely in freely suspended neutrophils when the molecular point attachments are not anchored to a stationary surface. Here, the cells rotate together and tensile and compressive forces vary rapidly and periodically in each orbit. Nevertheless, we occasionally observed rotation of doublets of cells, whose surfaces were separated by clear suspending fluid and apparently linked by an invisible flexible fiber. In these, the inter-particle distance varied with doublet orientation. As predicted by theory [42], for such a doublet, the period of rotation, T , at a given G , was significantly longer than that for a doublet of touching cells, indicating that the individual neutrophils were capable of independent rotation.

(e) Deformation and tether formation. Observations of neutrophils and other leukocytes rolling along vessel walls both *in vivo* and *in vitro* have shown that the cells are deformed with a section of flattened surface adhering to the wall [43-45]. Most of the work on the mechanics of rolling of leukocytes and the formation and break-up of the receptor ligand bonds, was carried out *in vitro* using a parallel plate flow chamber. These had a high ratio of width to height so that as the cells, observed using an inverted microscope, rolled on or were freely flowing near the lower surface, they traveled in a two-dimensional Poiseuille flow. In the meantime, it had become evident that, *in vivo*, the endothelial cells lining the walls of the post-capillary venules (and other blood vessels) have a layer, the glycocalyx also known as the endothelial surface layer (ESL), at the interface with the flowing blood. The thickness of the ESL is of the order of $0.4 - 0.5 \mu\text{m}$ [46]. The technique used to measure the glycocalyx thickness involved the use of high-resolution near-wall fluorescent micro-particle image velocimetry μ -PIV. Latex spheres of $0.47\text{-}\mu\text{m}$ diameter were injected into mouse cremaster muscle venules *in vivo* to measure velocity profiles in the red cell-depleted plasma layer near the

endothelial lining [46]. Since the glycocalyx thickness is somewhat greater than the mean resting length of the neutrophil microvillus ($0.3 \mu\text{m}$, [41]), the question arises how does the cell contact the endothelial cell membrane ligands that only extend $20\text{-}50 \text{ nm}$ above the plasma membrane through the ESL. The stiffness of the microvilli is thought to be insufficient to penetrate the ESL given the estimates of the hydraulic resistivity and restoring forces of the layer [46]. However, most leukocytes attach at the entrance of postcapillary venules having just passed through a channel of diameter smaller than its own where the leukocyte (deformed into a cylinder) is tightly squeezed against the capillary wall. As it exits the capillary, the red cells behind it having been held up by the slower velocity of the leukocyte, push past it thereby displacing it toward the venular wall, a mechanism modeled *in vitro* and seen *in vivo* [47]. If the leukocyte membrane is then squeezed against the venular wall, initial bonds can form and the tension in the selectin bond may be sufficient to overcome the restoring force of the glycocalyx [46]. Also, there is evidence that the ESL can change its properties in inflammation [48,49] and facilitate rolling and adhesion of leukocytes.

Recently, there have been reports of interesting work on neutrophil rolling using dynamic total internal reflection fluorescence microscopy (TIRFM) that can measure the topography of cell-substratum distances [50-52]. Blood from the carotid artery of a mouse flowed through a set of 9 parallel polydimethylsiloxane (PDMS) rectangular micro-channels and past a glass surface coated with P-selectin. Neutrophils were detected rolling along the P-selectin surface due to formation and breakage of P-selectin-PSGL-1 bonds. With the aid of a TIRFM microscope at very high magnification and appropriate fluorescence labeling of the neutrophils, distances between the microvillus and the P-selectin surface were estimated. After initial bond formation at resting lengths of 70 nm the microvilli at the leading end of the cell were compressed to within 25 nm near the cell center. At the trailing edge the bonds were stretched to lengths of $125\text{-}150 \text{ nm}$ before they broke away. Rolling at wall shear stresses as high as 0.6 Pa were stabilized by the formation of 3 to 4 long tethers that could remain bound to the substrate for 1 to 10 s and extended up to $16 \mu\text{m}$ behind the rolling cells.

5 NANO RHEOLOGY

5.1 Fluorescent particles in fluids and cells

In their paper on “Particle Tracking Microrheology of Complex Fluids” in *Physical Review Letters* (1997), the group at Johns Hopkins University wrote:

“In this letter we demonstrate that microscopic tracking of the thermally driven motion of a single particle suspended in a complex fluid can be used to measure the fluid’s macroscopic linear viscoelasticity over an extended frequency range. By extracting the particle’s time dependent

mean square displacement, $\langle \Delta r^2(t) \rangle$, from its trajectory measured using laser deflection particle tracking (LDPT), we obtain the stress relaxation modulus $G_r(t)$ from a frequency-dependent form of the Stokes-Einstein equation," [53].

That is indeed microrheology, and at the nanometer level. The technique of introducing nano-sized fluorescent particles into cells to measure the viscoelastic properties of cytoplasm locally and with high spatiotemporal resolution has become established [54]. It has the advantage over other single-cell mechanics (e.g. AFM) in that it avoids direct contact between the cell surface and the physical probe. Moreover, by tracking multiple beads simultaneously [55], one can measure the micromechanical responses to stimuli in different parts of the cell at the same time and over periods much shorter than those in tracking methods that correlate the motions between two beads [56].

5.2 Nanotubes as biomaterials

An interesting example of the use of nanostructures to direct the differentiation of human mesenchymal stem cells (hMSC) into osteoblasts was recently reported [57]. Nanotubes with titanium dioxide (TiO₂) surface structures and diameters from 30 to 100 nm were prepared. Cells were cultured on their surface to determine how the size of the tubes influenced the cellular response and differentiation. Cells were also cultured on flat TiO₂ surfaces. The results revealed a very dramatic change in hMSC behavior over a narrow range of nanotube dimension. Cells on flat TiO₂ remained rounded, cells in the 30 nm diameter tubes promoted adhesion without significant differentiation whereas the largest diameter nanotubes promoted a dramatic stem cell elongation with an accompanying cytoskeletal stress and selective differentiation into osteoblast-like cells.

It is significant that differentiation of the cells was achieved without additional biochemical inducing agents. Moreover, the TiO₂ nanotube long range structures were not patterned or highly ordered, but they do have their own robust and discrete nanotube shape [58]. It has also been reported that MSC cultured on highly nanopatterned poly(methylmethacrylate) (PMMA) surfaces did not exhibit osteogenic differentiation, whereas when cultured on PMMA with random patterned topography, osteoblastic morphology was promoted after 21 days incubation with cell growth media [59].

CONCLUDING REMARKS

It has been a long journey from Stanley Mason's first papers on *Particle Motions in Sheared Suspensions* from the Pulp and Paper Research Institute at McGill University in Montreal to present day micro- and nanotechnology and basic research. To have lived through the evolution of experimental and theoretical microrheological research, and to have been able to contribute a little to it has been a real privilege. None of this would have been possible without the support and dedication of technicians and graduate students. To all of you, I extend a heartfelt thank you. Your names as well as those of my collaborators will be found as co-authors in the publications listed below.

References

- [1] Goldsmith, H. L., and Mason, S. G., 1967, "The Microrheology of Dispersions," *Rheology: Theory and Applications*, Vol. IV, (F. R. Eirich, ed.), Academic, New York.
- [2] Trevelyan, B. J., and Mason, S. G., 1951, "Particle Motions in Sheared Suspensions. I. Rotations," *J. Colloid Sci.*, **6**, pp. 351-367.
- [3] Manley, R. St. J., and Mason, S. G. 1952, "Particle Motions in Sheared Suspensions. II. Collisions of Uniform Spheres," *J. Colloid Sci.*, **7**, pp. 354-369.
- [4] Mason, S. G., and Manley, R. St. J. 1956, "Orientations and Interactions of Rigid Rods," *Proc. R. Soc. (London)*, **A 238**, pp. 117-131.
- [5] Rumscheidt, F. D., and Masons, S. G., 1960, "Particle Motions in Sheared Suspensions XII. Deformation and burst of fluid drops in shear and hyperbolic flow," *J. Colloid Sci.*, **16**, pp. 238-261.
- [6] Goldsmith, H. L., and Mason, S. G., 1962, "The Flow of Suspensions Through Tubes. I. Single Spheres, Rods and Discs," *J. Colloid Sci.*, **17**, pp. 448-476.
- [7] Karnis, A., Goldsmith, H. L., and Mason, S. G., 1963, Axial Migration of Particles in Poiseuille Flow, *Nature*, **200**, pp. 159-160.
- [8] Goldsmith, H. L., and Marlow, J., 1972, "Flow Behaviour of Erythrocytes. I. Rotation and Deformation in Dilute Suspensions," *Proc. Roy. Soc. (London)*, **B 181**, pp. 351-384.
- [9] Vadas, E. B., Goldsmith, H. L., and Mason, S. G., 1973, "The Microrheology of Colloidal Dispersions I. The Microtube Technique," *J. Colloid Interface Sci.*, **43**, pp. 630-648.
- [10] Goldsmith, H. L., and Mason, S. G., 1962, "Particle Motions in Sheared Suspensions XIII. The Spin and Rotation of Discs," *J. Fluid Mech.*, **12**, pp. 88-96.
- [11] Schmid-Schönbein, H. and Wells, R., 1969, "Fluid Drop-Like Transition of Erythrocytes Under Shear," *Science*, **165**, pp. 228-231.
- [12] Keller, S. R., and Skalak, R., 1982, "Motion of a Tank-Treading Ellipsoidal Particle in a Shear Flow," *J. Fluid Mech.*, **120**, pp. 27-47.
- [13] Forgacs, O. L., and Mason, S. G. 1959, "Particle Motions in Sheared Suspensions. X. Orbits of Flexible Threadlike Particles," *J. Colloid Sci.*, **14**, pp. 473-491.
- [14] Goldsmith, H. L., and Mason, S. G., 1964, "The Flow of Suspensions Through Tubes. III. Collisions of small uniform spheres," *Proc. Roy. Soc. (London)*, **A 282**, pp. 569-591.
- [15] Karnis, A., and Mason, S. G., 1967, "Particle Motions in Sheared Suspensions XVIII. Wall Migration of Fluid Drops," *J. Colloid Interface Sci.*, **24**, 164-169.
- [16] Goldsmith, H. L., 1971, "Red Cell Motions and Wall Interactions in Tube Flow," *Fed. Proc.*, **30**, pp. 1578-1588.
- [17] Segré, G. and Silberberg, A., "The Behaviour of Macroscopic Rigid Spheres in Poiseuille Flow II. Experimental Results and Interpretations," 1962, *J. Fluid Mech.*, **14**, pp. 136-157.
- [18] Karnis, A., Goldsmith, H. L., and Mason, S. G. 1966, "The Flow of Suspensions Through Tubes. V. Inertial Effects," *Can. J. Chem. Eng.*, **44**, pp. 181-193.
- [19] Goldsmith, H. L., and Marlow, J., 1979, "Flow Behaviour of Erythrocytes. II. Particle Motions in Concentrated Suspensions of Ghost Cells," *J. Colloid Interface Sci.*, **71**, pp. 383-407.
- [20] Gauthier, F. P., Goldsmith, H. L., and Mason, S. G., 1972, "Flow of Suspensions Through Tubes. X. Liquid Drops as Models of Erythrocytes," *Biorheology*, **9**, pp. 205-224.
- [21] Vadas, E. B., Goldsmith, H. L., and Mason, S. G., 1976, "The Microrheology of Colloidal Dispersions. III. Concentrated Emulsions," *Trans. Soc. Rheol.*, **20**, pp. 373-407.
- [22] Karnis, A., Goldsmith, H. L., and Mason, S. G., 1966, "The Kinetics of Flowing Dispersions I. Concentrated Suspensions of Rigid Particles," *J. Colloid Interface Sci.*, **22**, pp. 513-553.
- [23] Skalak, R., 1992, An Interpretation of Partial Plug Flow of Concentrated Suspensions, *Biorheology*, **29**, pp. 479-488, 1992.
- [24] Goldsmith, H. L., and Skalak, R., 1975, *Ann. Rev. Fluid Mech.*, **7**, pp. 213-247.

- [25] Turitto, V. T., Benis, A. M., and Leonard, E. F., 1972, "Platelet Diffusion in Flowing Blood," *Ind. Eng. Chem. Fundam.*, **11**, pp. 216-223.
- [26] Cokelet, G. R., and Goldsmith, H. L., 1991, "Decreased Hydrodynamic Resistance in the Two-Phase Flow of Blood Through Small Vertical Tubes at Low Flow Rates," *Circ. Res.*, **69**, pp. 1-17.
- [27] Takamura, K., Goldsmith, H. L., and Mason, S. G., 1981, "The Microrheology of Colloidal Dispersions IX. Effects of Simple and Polyelectrolytes on Rotation of Doublets of Spheres," **72**, pp. 385-400.
- [28] Takamura, K., Goldsmith, H. L., and Mason, S. G. 1981, "The Microrheology of Colloidal Dispersions XII. Trajectories of Orthokinetic Pair-Collisions of Latex Spheres," *J. Colloid Interface Sci.*, **83**, pp. 516-530.
- [29] van de Ven, T. G. M., and Mason, S. G., 1976, "The Microrheology of Colloidal Dispersions IV. Pairs of Interacting Spheres in Shear Flow," *J. Colloid Interface Sci.*, **57**, pp. 505-516.
- [30] Arp, P. A., and Mason, S. G., 1977, "The Kinetics of Flowing Dispersions. VIII. Doublets of Rigid Spheres (Theoretical)," *J. Colloid Interface Sci.*, **62**, pp. 21-43.
- [31] Tha, S. P., and Goldsmith, H. L. 1986, "Interaction Forces Between Red Cells Agglutinated by Antibody. I. Theoretical," *Biophys. J.*, **50**, pp. 1109-1116.
- [32] Goldsmith, H. L. 1996 "The Microrheology of Dispersions: Application to Blood Cells," *Jap. J. Biorheology*, **10**, pp. 155-176.
- [33] Schmid-Schönbein, H., Wells, R., and Schildkraut, R., 1969, "Microscopy and viscometry of blood under uniform shear rate (rheoscopy)," *J. Appl. Physiol.*, **26**, pp. 674-678.
- [34] Tees, D. F. J., Coenen, O., and Goldsmith, H. L. 1993, "Interaction Forces Between Red Cells Agglutinated by Antibody IV. Time and Force of Break-up," *Biophys. J.*, **65**, pp. 1318-1334.
- [35] Tees, D. F. J., and Goldsmith, H. L. 1996, "Kinetics and Locus of Failure on of Receptor-Ligand-Mediated Adhesion Between Latex Spheres I. Protein-Carbohydrate Bond," *Biophys. J.*, **71**, pp. 1102-1114.
- [36] Simon, S. I., Chambers, J. D., and Sklar, L. A. 1990, "Flow cytometric Analysis and Modeling of Cell-Cell Adhesive Interactions: the Neutrophil as a model," *J. Cell. Biol.*, **111**, pp. 2747-2756.
- [37] Goldsmith, H. L., Quinn, T. A., Drury, G., Spanos, C., McIntosh, F. A. and Simon, S. I. 2001, "Dynamics of Neutrophil Aggregation in Couette Flow Revealed by Videomicroscopy: Effect of Shear Rate on Two-Body Collision Efficiency and Doublet Lifetime," *Biophys. J.*, **81**, pp. 2020-2034.
- [38] Evans, E., Leung, A., Hammer, D., and Simon, S. I., 2001, "Chemically Distinct Transition States Govern Rapid Dissociation of Single L-Selectin Bonds Under Force," *Proc. Natl. Acad. Sci. U.S.A.*, **98**, pp. 3784-3789.
- [39] Evans, E., and A, Leung, 1989, "Apparent Viscosity and Cortical Tension of Blood Granulocytes Determined by Micropipet Aspiration," *Biophys. J.*, **56**, pp. 151-160.
- [40] Bruehl, R. E., Springer, T. A., and Bainton, D. F. 1996, "Quantitation of L-Selectin Distribution on Human Leukocyte Microvilli by Immunogold Labeling and Electron Microscopy," *J. Histochem. Cytochem.*, **44**, pp. 835-844.
- [41] Shao, J.-Y., Ting-Beall, H. P., and Hochmuth, R. M., 1998, "Static and Dynamic Lengths of Neutrophil Microvilli," *Proc. Nat. Acad. Sci. U.S.A.*, **95**, pp. 6797-6802.
- [42] Takamura, K., Adler, P. M., Goldsmith, H. L., and Mason, S. G., 1981, "Particle Motions in Sheared Suspensions XXXI. Rotations of Rigid and Flexible Dumbbells (Experimental)," *J. Colloid Interface Sci.*, **83**, pp. 516-530.
- [43] Firrell, J., and Lipowsky, H. H., 1989, "Leukocyte Margination and Deformation in Mesenteric Venules of Rat," *Am. J. Physiol. Heart. Circ. Physiol.*, **256**, pp. H1667-H1674.
- [44] Damiano, E. R., Westheider, J., Tozeren, A., and Ley, K., 1996, "Variation in the Velocity, Deformation and Adhesion Energy Density of Leukocytes Rolling Within Venules," *Circ. Res.* **79**, pp. 1122-1130.
- [45] Smith, M. L., Smith, M. M., Lawrence, M. B., and Ley, K. 2002, "Viscosity-Independent Velocity of Neutrophils Rolling on P-Selectin In Vitro or In Vivo," *Microcirculation*, **9**, pp. 523-536.
- [46] Smith, M. L., Long, D. L., Damiano, E. R., and Ley, K., 2003, "Near-Wall μ -PIV Reveals a Hydrodynamically Relevant Endothelial Surface Layer in Venules in Vivo," *Biophys. J.*, **85**, pp. 637-645.
- [47] Schmid-Schönbein, G. W., Usami, S., Skalak, R., and S. Chien, 1980, "The Interaction of Leukocytes and Erythrocytes in Capillary and Postcapillary Vessels," *Microvasc. Res.*, **19**, pp. 45-70.
- [48] Vink, H., Constantinescu, A. A. and Spaan, J. A., 2000, "Oxidized Lipoproteins Degrade the Endothelial Surface Layer: Implications for Platelet Endothelial Cell Adhesion," *Circulation*, **101**, pp. 1500-1502.
- [49] Mulivor, A. W., and Lipowsky, H. H., 2002, "Role of Glycocalyx in Leukocyte-Endothelial Cell Adhesion," *Am. J. Physiol. Heart Circ. Physiol.*, **283**, pp. H1282-H1291.
- [50] Sundd, P., Gutierrez, E., Pospieszalska, A., and Ley, K., 2010, "Stressed Microvilli and Long Tethers in Rolling, Light Adhesion Zones and Aft Trunks in Arresting Neutrophils Revealed Using Total Internal Reflection Microscopy," *Experimental Biology*, Anaheim, CA, page 163 (Abstract).
- [51] Truskey, G. A., Burmeister, J. S., Grapa, E., and Reichert, W. M. 1992, "Total Internal Reflection Fluorescence Microscopy (TIRFM) II. Topographical Mapping of Relative Cell/Substratum Separation Distances," *J. Cell. Sci.* **103**, pp. 491-499.
- [52] Pospieszalska, M. K., and Ley, K., 2009, "Dynamics of Microvillus Extension and Tether Formation in Rolling Leukocytes," *Cell. Molec. Bioeng.* **2**, pp. 207-217.
- [53] Mason, T. G., Ganesan, K., van Zanten, J. H., Wirtz, D., and Kuo, S. C., 1997, "Particle Tracking Microrheology of Complex Fluids," *Phys. Rev. Lett.*, **79**, pp. 3282-3285.
- [54] Wirtz, D. "Particle-Tracking Microrheology of Living Cells: Principles and Applications," 2009, *Annu. Rev. Biophys.* **38**, pp. 301-326.
- [55] Tseng, Y., Kole, T. P., and Wirtz, D. 2002, "Micromechanical Mapping of Live Cells by "Multiple-Particle-Tracking Microrheology," *Biophys. J.*, **83**, pp. 3162-3176.
- [56] Crocker J. C., Valentine M. T., Weeks E. R. et al. 2000, "Two-Point Microrheology of Inhomogeneous Soft Materials," *Phys. Rev. Lett.* **85**, pp.888-891.
- [57] Oh, S., Brammer, K. S., Li, Y. S. J. et al., 2009, "Stem Cell Fate Dictated Solely by Altered Nanotube Dimension," *Proc. Natl. Acad. Sci. U.S.A.*, **106**, pp. 2130-2135.
- [58] Oh, S., Daraio, C., Chen, L-H, et al., 2006, "Significantly Accelerated Osteoblast Growth on Aligned TiO₂ nanotubes," *J. Biomed. Mater. Res.*, **A 78**, pp. 97-103.
- [59] Dalby, M. J., Gadegaard, N., Tare, R. et al., 2007, "The Control of Human Mesenchymal Cell Differentiation Using Nanoscale Symmetry and Disorder," *Nat. Mater.*, **6**, 997-1003.